Dyes and Pigments 88 (2010) 174–179

Contents lists available at ScienceDirect

Dyes and Pigments

journal homepage: www.elsevier.com/locate/dyepig

# Organic/polyoxometalate hybridization dyes: Crystal structure and enhanced two-photon absorption

Jieying Wu [a,b,*], Guiju Hu [a], Peng Wang [a], Fuying Hao [a], Hongping Zhou [a], Aimin Zhou [a], Yupeng Tian [a,b,c], Baokang Jin [a,b,*]

[a] Department of Chemistry, Key Laboratory of Functional Inorganic Materials of Anhui Province, Anhui University, 230039 Hefei, PR China
[b] State Key Laboratory of Crystal Materials, Shandong University, Jinan 250100, PR China
[c] State Key Laboratory of Coordination Chemistry, Nanjing University, Nanjing 210093, China

ARTICLE INFO

*Article history:*
Received 8 April 2010
Received in revised form
4 June 2010
Accepted 9 June 2010
Available online 16 June 2010

*Keywords:*
POM Dye
Polyoxometalate
Single crystal
Fluorescence
Two-photon absorption

ABSTRACT

The structures of four novel organic–inorganic hybrid dyes, namely *trans*-4-(4′-(*N*,*N*-Dialkylaminostyryl))-*N*-Methyl-pyridinium[$Mo_6O_{19}^{2-}$] [alkyl = Et(**POM1**), Pr(**POM2**), *n*-Bu(**POM3**) and Me, hydroxyethyl(**POM4**)], were characterized by single crystal *X*-ray diffraction analysis. Hybridization of the organic chromophores with polyoxometalate enhanced their two-photon absorption cross sections and thermal stability. The linear optical properties of the hybrid dyes were investigated using absorption and fluorescence spectra in both the solution and solid states. The two-photon absorption cross section $\delta$ and coefficient $\beta$ were obtained using the *Z*-scan technique. Correlations between dye structure and optical property were investigated.



## 1. Introduction

Two-photon absorption (TPA), a third-order nonlinear optical process in which two photons are simultaneously absorbed to an excited state in a medium via a virtual state [1], has enjoyed much attention recently owing to its interesting two-photon pumped frequency up-conversion (TPP) mechanism and exciting applications that vary from optical limiting [2–5] to three-dimensional (3D) fluorescence microscopy [6–9], 3D microfabrication [10,11], optical data storage [12,13], photoacid generation [14,15], photodynamic therapy [16,17], and bioimaging [18,19]. Recent studies [20–27] have shown design strategies for efficient TPA molecules based on systematic investigations of chromophores with various electron-donor and electron-acceptor moieties, which are attached symmetrically or asymmetrically to a conjugated linker ($\pi$-center). Interest in dyes over the last 30 years has occurred because many derivatives possess large second-order molecular hyperpolarizability [28–36]. However, the synthesis of most organic molecules with strong TPA properties is complex and generally affords compounds in very low yield.

Recently, organic–inorganic hybrids have attracted substantial attention [37–39]. In comparison with small organic molecules, organometallic compounds usually show superior secondary (i.e., physical, thermal and mechanical) properties, which are important for material processing and device fabrication. Tian and co-workers [40–42] reported that pyridinium salts can combine with different functional inorganic moieties to furnish a series of novel hybrid dyes bearing higher two-photon across sections compared to those of the starting materials.

It is well known that polyoxometalates are extremely versatile inorganic building blocks for the construction of molecule-based materials [43–45]. Therefore, we widened our research area based on the previous work of our group, polyoxometalates metathesis have been successfully used to prepare four novel inorganic-organic hybrid dyes as well, **POM1**, **POM2**, **POM3** and **POM4**, from different pyridinium salts. The hybrid dyes exhibit higher stability that enough to undergo strong laser pulses. The TPA properties of them in DMF (dimethyl formamide) were studied by *Z*-scan technique [46]. Both the TPA coefficient $\beta$ and TPA cross-section $\delta$ have been obtained in order to investigate correlations between molecular structure and third-order nonlinear property [47].

* Corresponding authors. NO. 3 Fei Xi Road, HeFei, An Hui 230039, China. Tel.: +86 5515108151; fax: +86 5515107342.
*E-mail addresses:* jywu1957@163.com (J. Wu), bkjinhf@yahoo.com.cn (B. Jin).

0143-7208/$ – see front matter © 2010 Elsevier Ltd. All rights reserved.
doi:10.1016/j.dyepig.2010.06.004

## 2. Experimental

### 2.1. Apparatus and materials

All chemicals and solvents were dried and purified by usual methods. Elemental analyses were performed with a Perkin–Elmer 240C elemental analyzer. IR spectrums were recorded with a Nicolet FT-IR Nexus 870 instrument in the range 4000–400 $cm^{-1}$ by using KBr pellets. Fig. 1 shows the typical linear absorption spectra of the four POMs in DMF with the concentration of $1 \times 10^{-5}$ mol/L, recorded on Perkin Elmer spectrophotometer. Both solid and solution fluorescence spectra (The concentrations of DMF is $1 \times 10^{-5}$ mol/L.) of the four POMs were measured in the same Perkin Elmer LS50B fluorophotometer. The single excited maximum is around 460 m, and the single emission is about 640 nm (Figs. 2 and 3, respectively). TPA cross sections were measured by *Z*-scan technique with ns-laser source (Fig. 4). The pump source was a Q-switched and frequency-doubled Nd:YAG laser ($\lambda = 1064$ nm) with a 19 ns pulse width (produced by Hefei Institutes of Physical Science, Chinese Academy of Sciences) and 1 Hz repetition rate. The samples dissolved in DMF at the concentration of $1 \times 10^{-3}$ mol/L were placed in an optical quartz cuvettes with a 1 mm path length. Thermogravimetric analysis was performed on the solid sample in the range of 20–600 °C under nitrogen (Fig. 5).

### 2.2. Synthesis

All the dyes were synthesized as described previously [48] (Scheme 1). **Dye1**, **Dye2**, **Dye3** and **Dye4** were converted to **POM1**, **POM2**, **POM3** and **POM4** almost quantitatively by ion exchanging between dyes and polyoxometalates.

**POM1**: 1.16 g (2.45 mmol) of $Na_2MoO_4 \cdot 2H_2O$ was added to 5 mL DMF and the solution was heated to 40 °C for 10 min with stirring. 1 mL acetic anhydride was added slowly with stirring over 5 min. 1 mL $HNO_3$ was added very slowly and a bright yellow solution formed. The ensuing solution was stirred for another 10 min and filtered. 0.80 g (2 mmol) **Dye1** dissolved in 3 mL DMF was added to the filtrate slowly, forming a gray solid immediately. The solid was collected by filtration and washed with ethanol and ethyl ether, yield 1.72 g (96.5%). IR date (KBr discs, $cm^{-1}$): 3430 (vs), 1646 (m), 1577 (s), 1524 (s), 1406 (w), 1319 (w), 1270 (w), 1177 (vs), 1153 (vs), 956 (vs), 796 (vs). Anal. Calcd for $C_{36}H_{46}Mo_6N_4O_{19}$: C, 30.57; H, 3.28; N, 3.96%. Found: C, 30.54; H, 3.27; N, 3.95%.

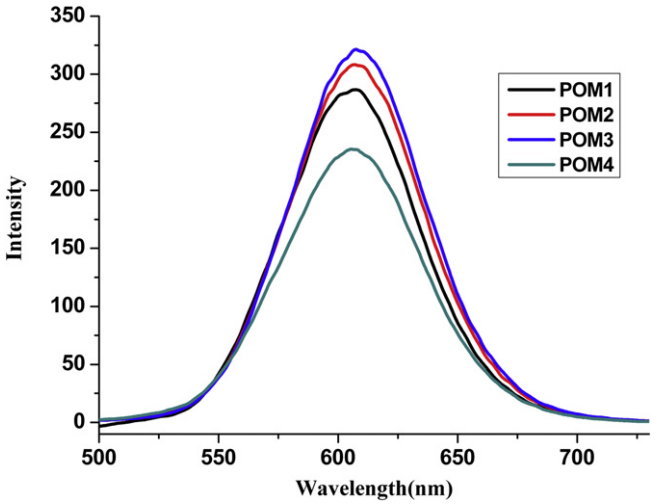


**Fig. 2.** The fluorescent spectra of POMs in DMF with $1 \times 10^{-5}$ mol/L.

**POM2**: This was prepared by a procedure similar to **POM1** except that **Dye1** was replaced by **Dye2**. IR date (KBr discs, $cm^{-1}$): 3567 (vs), 2934 (m), 1793(w), 1647 (w), 1577 (m), 1523 (m), 1340 (w), 1177 (vs), 952 (m), 875 (w), 794 (m), Anal. Calcd for $C_{40}H_{54}Mo_6N_4O_{19}$: C, 32.67; H, 3.70; N, 3.81%. Found: C, 32.64; H, 3.69; N, 3.79%.

**POM3**: This was prepared by a procedure similar to **POM1** except that **Dye1** was replaced by **Dye3**. IR date (KBr discs, $cm^{-1}$): 3566 (vs), 2928 (s), 2366 (w), 1793 (w), 1647 (m), 1577 (m), 1541(m), 1523 (m), 1508 (m), 1458 (v), 1176 (s), 952 (s), 795 (s). Anal. Calcd for $C_{44}H_{62}Mo_6N_4O_{19}$: C, 31.33; H, 3.71; N, 3.32%. Found: C, 31.60; H, 3.52; N, 3.67%.

**POM4**: The same synthesis procedure as for **POM1** was used except that **Dye1** was replaced by **Dye4**. IR date (KBr discs, $cm^{-1}$): 3448 (vs), 2920 (m), 2851 (m), 1644(w), 1576(vs), 1524 (vs), 1459 (w), 1382(m), 1315(m), 1171(vs), 958 (vs), 795 (vs), 600 (w). Anal. Calcd for $C_{34}H_{42}Mo_6N_4O_{21}$: C, 28.79; H, 2.98; N, 3.95%. Found: C, 28.75; H, 2.99; N, 3.96%.

### 2.3. X-ray crystallography

Date collections were performed using Siemens SMART CCD area detector diffractometer with $MoK_\alpha$ radiation with an ω-scan

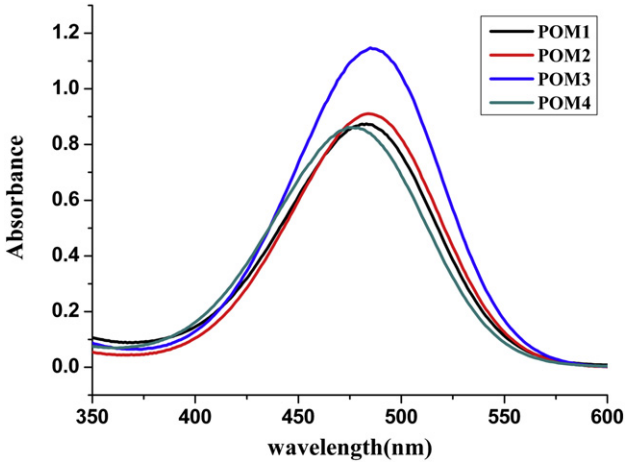


**Fig. 1.** The absorption spectra of POMs in DMF with $1 \times 10^{-5}$ mol/L.

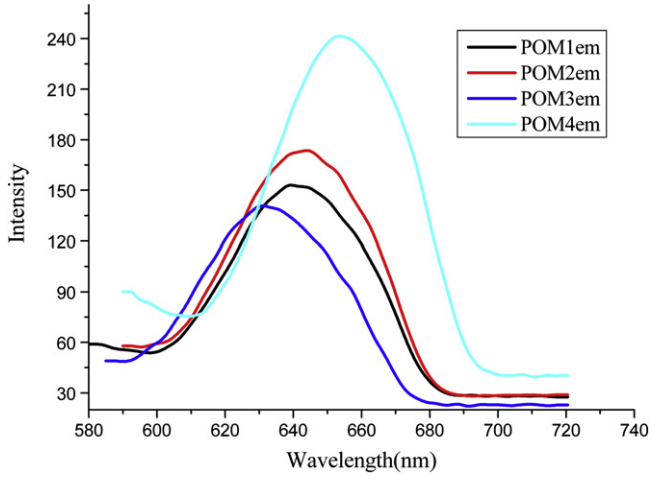


**Fig. 3.** The fluorescent spectra of POMs in solid state.

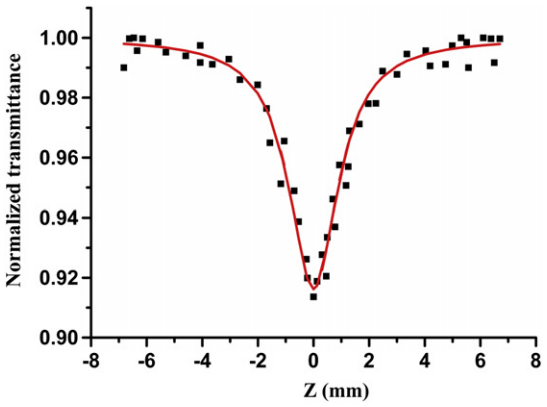


**Fig. 4.** *Z*-scan data for POM2 at 1064 nm.

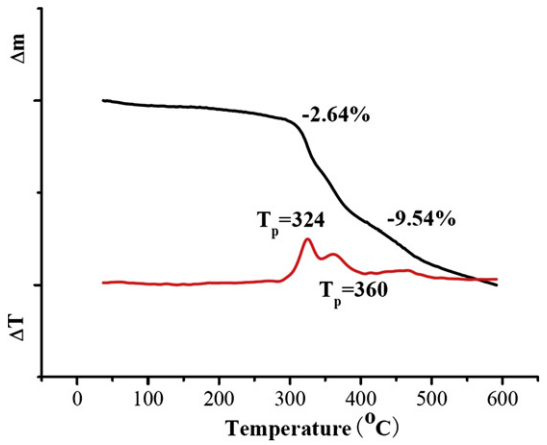


**Fig. 5.** TGA-TG curve for the **POM1.** The solid curves are theoretical fits of the experimental data.

mode ($\lambda$ = 0.71073 Å). The structures were solved with direct methods using the SHELXTL program and refined anisotropically with SHELXTL using full-matrix least squares procedure [49]. All non-hydrogen atoms were refined anisotropically. The crystallographic data for compounds **POM1**, **POM2** and **POM4** are listed in Table 1 (in supporting information) (Fig. 6 shows the plot of the unit of **POM1**, **POM2** and **POM4**). Selected bond lengths and angles for **POM1**, **POM2** and **POM4** are presented in Table 2. CCDC No. 618508 for **POM1**, No. 618510 for **POM2** and No. 618509 for **POM4**.

## 3. Results and discussion

Both single crystals of **POM1** and **POM2** were prepared by diffusing isopropanol into DMF solution. For **POM4**, crystals

**Table 1**
Crystallographic data and structure refinement for compounds **POM1**, **POM2** and **POM4**.

| Compound | POM1 | POM2 | POM4 |
|---|---|---|---|
| Chemical formula | $C_{36}H_{46}Mo_6N_4O_{19}$ | $C_{40}H_{54}Mo_6N_4O_{19}$ | $C_{34}H_{42}Mo_6N_4O_{21}$ |
| Formula weight | 1414.41 | 1470.51 | 1418.36 |
| Crystal system | Monoclinic | Triclinic | Monoclinic |
| Space group | $P2_1/c$ | $P-1$ | $P2_1/c$ |
| $a$ (Å) | 8.1819(1) | 13.3330(4) | 8.1431(1) |
| $b$ (Å) | 18.3024(2) | 13.5313(4) | 18.3901(3) |
| $c$ (Å) | 15.5081(2) | 13.9416(5) | 15.2426(2) |
| $\alpha$ (°) | 90 | 87.419(1) | 90 |
| $\beta$ (°) | 103.225(1) | 76.318(1) | 103.378(1) |
| $\gamma$ (°) | 90 | 89.415(1) | 90 |
| $V$ (Å$^3$) | 2260.72(5) | 2441.39(14) | 2220.68(5) |
| $Z$ | 2 | 2 | 2 |
| $M$ (mm$^{-1}$) | 1.693 | 2.000 | 2.115 |
| Reflections collected | 13 615 | 15 019 | 13 287 |
| Reflections [$I \geq 2\sigma(I)$] | 5481 | 11 280 | 5352 |
| $R_1$, $wR_2$ [$I \geq 2\sigma(I)$] | 0.0500, 0.1087 | 0.0645, 0.1558 | 0.0680, 0.1205 |
| $R_1$, $wR_2$ [all data] | 0.0744, 0.1151 | 0.0903, 0.1892 | 0.0680, 0.1205 |
| Goodess-of-fit on $F^2$ | 0.945 | 0.935 | 1.029 |
| Largest peak and hole ($e$ Å$^3$) | 1.073, −1.941 | 1.633, −2.428 | 1.179, −2.029 |

suitable for *X*-ray diffraction analysis were obtained by diffusing ethanol into concentrated DMF solution. ORTEP views for the three crystal structures were shown in Fig. 1. From Table 2, the bond lengths of C(6)–C(7) for **POM1**, C(6)–C(7) for **POM2** and C(7)–C(8) for **POM4** are 1.340, 1.355 and 1.340, respectively, indicating that the cations possess conjugated configuration, which is favourable to molecule hyperpolarizabilities according to the idea of Marder et al. [50].

All the structures have similar characters, the cations contact with the anions not only by electrostatic attraction, but also by C–H···O hydrogen bonds and the intermolecular interaction between the cations involves π–π stacking interactions.

From Fig. 3, thermogravimetric analyses (TGA) show that **POM1** lost 2.64% of the total weigh at 324 °C, corresponding to the loss of $-C_2H_5$ group per formula. Further heating leads to another $-C_2H_5$ group loss in mass of about 9.99%. For comparison, the decomposed temperatures of the corresponding iodides were also listed in Table 3.[49] It is clearly to see that almost all the polyoxometalates are more stable than iodides. The ionic interactions between the methylpyridinium cations and their corresponding anions are almost the same in the two materials, it is hydrogen bonds (C–H···O interaction) that plays an important role in enhancement of thermal stability. Although the C–H···O interaction is very weak in the crystal, but the same methylpyridinium cation interacts with different anions through four or more, so the enhancement of the decomposed temperature is easily to be understood. Table 4 shows us the detailed information of hydrogen bonds in the crystal of **POM1**, **POM2** and **POM4**.

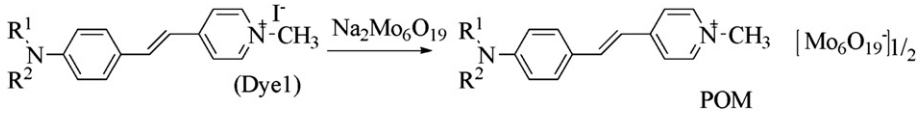


POM1 ( $R^1 = R^2$ = Ethyl )
POM2 ( $R^1 = R^2$ = n-propyl )
POM3 ( $R^1 = R^2$ = n-butyl )
POM4 ( $R^1$ = Hydroxy ethyl, $R^2$ = Methyl )

**Scheme 1.** Synthesis of **POM1**, **POM2**, **POM3** and **POM4**.

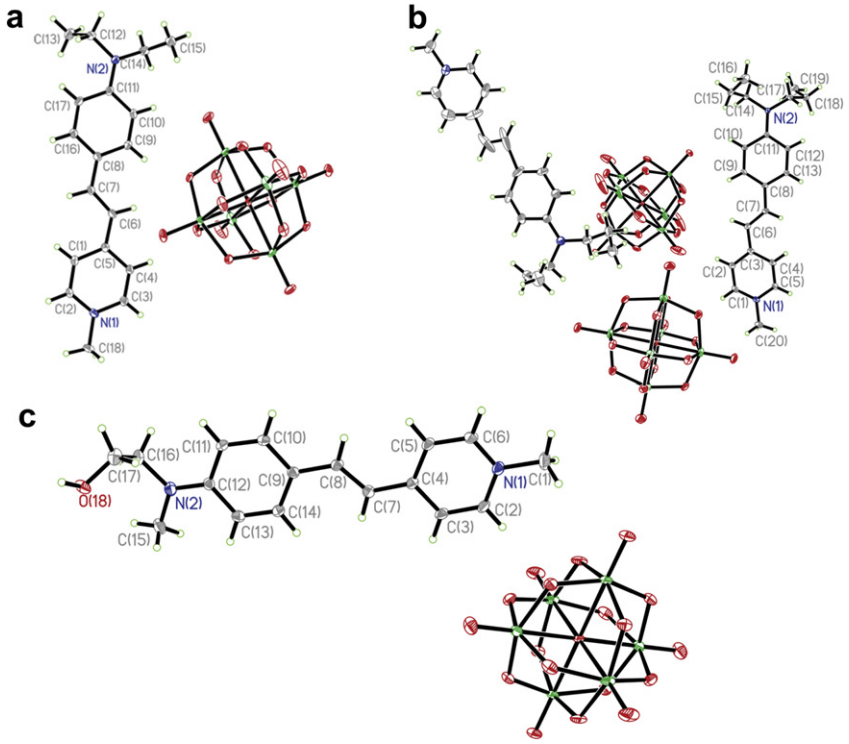


**Fig. 6.** (a) ORTEP plot of the unit of **POM1**. (b) ORTEP plot of the unit of **POM2**. (c) ORTEP plot of the unit of **POM4** (Crystallographic numbering).

Table 5 shows the absorption peaks at 483 nm for **POM1** (with the corresponding mole absorption coeffient $\varepsilon = 8.74 \times 10^4$), 484 nm for **POM2** ($\varepsilon = 9.10 \times 10^4$), 485 nm for **POM3** ($\varepsilon = 1.14 \times 10^5$), and 474 nm for **POM4** ($\varepsilon = 8.62 \times 10^4$), respectively.

**Table 2**
Selected bond lengths (Å) and angles (°) for **POM1**, **POM2** and **POM4**.

| | | | |
|---|---|---|---|
| **POM1** | | | |
| C(5)–C(6) | 1.451(6) | C(9)–C(8)–C(7) | 122.6(5) |
| C(6)–C(7) | 1.340(7) | C(6)–C(7)–C(8) | 126.6(5) |
| C(7)–C(8) | 1.446(6) | C(7)–C(6)–C(5) | 125.9(5) |
| C(1)–C(2) | 1.355(7) | C(1)–C(5)–C(6) | 124.1(5) |
| N(1)–C(2) | 1.349(6) | C(2)–C(1)–C(5) | 120.9(5) |
| N(1)–C(3) | 1.361(6) | N(1)–C(2)–C(1) | 121.5(4) |
| C(3)–C(4) | 1.349(7) | C(2)–N(1)–C(3) | 119.1(4) |
| C(4)–C(5) | 1.404(7) | C(4)–C(3)–N(1) | 121.2(5) |
| C(1)–C(5) | 1.400(6) | C(3)–C(4)–C(5) | 121.2(5) |
| | | C(1)–C(5)–C(4) | 116.1(5) |
| **POM2** | | | |
| C(4)–C(7) | 1.445(5) | C(8)–C(7)–C(4) | 125.2(4) |
| C(7)–C(8) | 1.339(5) | C(7)–C(8)–C(9) | 126.7(4) |
| C(8)–C(9) | 1.453(5) | C(10)–C(9)–C(8) | 120.1(4) |
| N(1)–C(2) | 1.354(6) | C(3)–C(4)–C(7) | 119.5(4) |
| C(2)–C(3) | 1.369(6) | C(2)–C(3)–C(4) | 120.5(4) |
| C(3)–C(4) | 1.406(5) | N(1)–C(2)–C(3) | 120.9(4) |
| C(4)–C(5) | 1.397(6) | C(6)–N(1)–C(2) | 119.9(4) |
| C(5)–C(6) | 1.361(6) | N(1)–C(6)–C(5) | 121.2(4) |
| N(1)–C(6) | 1.343(5) | C(6)–C(5)–C(4) | 121.0(4) |
| | | C(5)–C(4)–C(3) | 116.5(4) |
| **POM4** | | | |
| N(1)–C(1) | 1.345(8) | C(1)–N(1)–C(5) | 119.6(5) |
| N(1)–C(5) | 1.365(7) | N(1)–C(5)–C(4) | 120.3(6) |
| C(1)–C(2) | 1.374(9) | C(5)–C(4)–C(3) | 121.6(6) |
| C(2)–C(3) | 1.401(8) | C(4)–C(3)–C(2) | 116.5(6) |
| C(3)–C(4) | 1.391(9) | C(1)–C(2)–C(3) | 120.7(6) |
| C(4)–C(5) | 1.373(8) | N(1)–C(1)–C(2) | 121.4(6) |
| C(3)–C(6) | 1.444(8) | C(4)–C(3)–C(6) | 122.9(5) |
| C(6)–C(7) | 1.354(8) | C(7)–C(6)–C(3) | 123.2(6) |
| C(7)–C(8) | 1.446(8) | C(6)–C(7)–C(8) | 128.7(6) |

All the molecules are of D–π–A structures, those absorption bands could be safely attributed to CT (charge transfer). [51] There is no reasonable linear absorption in the spectral range from 600 to 1200 nm. Therefore, any absorption induced by excitation in this spectral range is due to a multi-photons process. From Table 5, we could easily obtain the information that the different alkyl chain attached to amino groups have influence on the absorption spectra, $\lambda_{max}$, which of the molecule with a long alkyl chain attached to amino groups exhibit more red-shift than one with a short, indicating that amino group with longer alkyl possess a little stronger electron-donating abilities than short one. With a little stronger electron-donating amino group, the $\lambda_{max}$ become red-shift and $\varepsilon$ become larger. But for the **POM4**, $\lambda_{max}$ and $\varepsilon$ is smallest among the four POMs. It can be easily understood that the hydroxyethyl group is a weaker donor than the alkyl group, for the strong electron-withdrawing abilities of the oxygen atom. And such order is also observed from the fluorescence data of the four POMs in solution shown in Table 5. But it is difficult to get the exact wavelength for that some peaks are widened. The trend of the relative intensity of

**Table 3**
TGA data of **POM1**, **POM2**, **POM3** and **POM4**.

| | Temp[a] (°C) | Lost mass (%) | Theoretical calculation (%) | | Temp[b] (°C) |
|---|---|---|---|---|---|
| **POM1** | 324 | 2.64 | 4.08 | $-C_2H_5$ | 264.7 |
| | 360 | 9.54 | 8.15 | $-C_4H_{10}$ | (ref[10]) |
| **POM2** | 309 | 0.73 | 5.82 | $-C_3H_7$ | |
| | 350 | 4.10 | 11.63 | $-C_6H_{17}$ | |
| **POM3** | 308 | 9.00 | 2.94 | $-C_4H_9$ | |
| | 394 | 15.00 | 5.06 | $-C_8H_{18}$ | |
| **POM4** | 290 | 3.30 | 2.21 | $-CH_3$ | 286.7 |
| | 430 | 10.20 | 8.40 | $-C_3H_8O$ | (ref[10]) |

[a] Decomposition temperature of the POMs.
[b] Decomposition temperature of the corresponding iodide dyes.

**Table 4**
Information of the hydrogen bonds.

| Donor–H···Acceptor[a] | D–H[Å] | H···A[Å] | D···A[Å] | D–H···A[°] |
|---|---|---|---|---|
| **POM1** | | | | |
| C2–H2A···O1#3 | 0.93 | 2.53 | 3.333 | 145 |
| C3–H3A···O7#4 | 0.93 | 2.5 | 3.2594 | 139 |
| C4–H4A···O8 | 0.93 | 2.41 | 3.2838 | 156 |
| C10–H10A···O2#1 | 0.93 | 2.53 | 3.2243 | 132 |
| C12–H12B···O5#2 | 0.97 | 2.51 | 3.331 | 142 |
| C18–H18B···O1#3 | 0.96 | 2.41 | 3.3065 | 155 |
| **POM2** | | | | |
| C1–H1A···O18#1 | 0.93 | 2.37 | 3.1436 | 141 |
| C5–H5B···O7#2 | 0.93 | 2.59 | 3.2016 | 124 |
| C7–H7B···O9#3 | 0.93 | 2.59 | 3.5064 | 167 |
| C10–H10A···O8 | 0.93 | 2.59 | 3.2037 | 124 |
| C25–H25A···O10 | 0.93 | 2.31 | 3.0472 | 136 |
| **POM4** | | | | |
| O18–H18A···O7#1 | 0.96 | 1.89 | 2.8135 | 162 |
| C1–H1A···O8#3 | 0.96 | 2.53 | 3.3848 | 149 |
| C2–H2A···O6 | 0.93 | 2.52 | 3.3213 | 145 |
| C3–H3A···O4 | 0.93 | 2.49 | 3.3014 | 146 |
| C5–H5B···O2#2 | 0.93 | 2.57 | 3.2614 | 131 |
| C6–H6B···O8#3 | 0.93 | 2.59 | 3.3264 | 137 |
| C8–H8A···O5#2 | 0.93 | 2.57 | 3.4534 | 159 |

[a] For **POM1**, #1: $-x$, $1-y$, $1-z$; #2: $-1+x$, $0.5-y$, $-0.5+z$; #3: $-1+$x, $0.5-y$, $-0.5+z$; #4: $-1+x$, $y$, $z$. For **POM2**, #1: $2-x$, $1-y$, $1-z$; #2: $2-x$, $1-y$, $-z$; #3: $-1+x$, $y$, $z$. For **POM4**, #1: $-2+x$, $y$, $-1+y$; #2: $-1+x$, $0.5-y$, $-0.5+z$; #3: $-x$, $-0.5+y$, $1.5-z$; #4: $-1+x$, $y$, $z$.

the four POMs is the same as that of their absorption spectra, which is 2Bu>2Pr>2Et > Me + $CH_2CH_2OH$, and consistent with their electron donating abilities.

Interestingly, the $\lambda_{em}$ exhibit different order, as shown in Figs. 2 and 3, owing to different their molecular configurations both in solid state and dilute solution. In the solution the interaction between the methylpyridinium cations and the polyoxometalate anions is so small that the energy of the excited spectra depends on the donor of the methylpyridinium cations. The stronger abilities the donors possess, the lower energy the excited state and the stronger intensity the emission band, and this is consistent with the results discussed above.

However, in the solid state, a broad red-shifted band fluorescence with maxima of 640, 645, 631 and 655 nm, respectively, indicates that the emission arises from the π-stacked aggregates [52–54]. The fluorescence spectrum of the POM3 shows only a small red-shifted when compared to the **POM1** and **POM2**, resulting from the largest interchain distance due to the long *n*-butyl chain of methylpyridinium cations. While the **POM4** is quite different from the others, it interacts with polyoxometalate by a strong hydrogen bond that is O18–H18A···O7#1, which is the strongest in all the three crystals. The distance between O18 and O7 is 2.8135 Å. The hydrogen-bonding formation will influence on the whole electron density distribution in the molecule, which is observed through its luminescent way [55]. And this strong hydrogen-bonding not only takes effect on the luminescence, but also on the TPA cross sections of the hybrid materials.

**Table 5**
The linear and nonlinear spectra of POM1, POM2, POM3 and POM4.

| | | POM1 | POM2 | POM3 | POM4 |
|---|---|---|---|---|---|
| Absorption spectra | $\lambda_{max}$ (nm) | 483 | 484 | 485 | 474 |
| | *A* | 0.87414 | 0.91087 | 1.14696 | 0.86215 |
| | $\varepsilon$ ($10^{-5}$) | 8.7414 | 9.1087 | 11.4696 | 8.6215 |
| Solution fluorescence | $\lambda_{ex}$ (nm) | 474 | 473[a] | 471[a] | 463 |
| | $\lambda_{em}$ (nm) | 607 | 606 | 609 | 607 |
| | Intensity | 290 | 310 | 350 | 240 |
| Solid fluorescence | $\lambda_{ex}$ (nm) | 462 | 460 | 456 | 473 |
| | $\lambda_{em}$ (nm) | 640 | 645 | 631 | 655 |
| Nonlinear optical properties[b] | ($\beta$)[c] Cm/GW | 0.2654 | 0.2503 | 0.2443 | 0.2789 |
| | ($\sigma$)[c] | 8233.28 | 7764.90 | 7578.64 | 8961.19 |
| | ($\sigma$)[d] | 7533.16 | 7233.34 | 7033.78 | 8033.46 |

[a] Widen peak.
[b] $10^{-50}$ $cm^4$s/photon.
[c] POM.
[d] Corresponding iodide.

It is well known to all that the TPA cross section $\delta$ value increases as the donor strength and conjugation length increases. At present work, the TPA cross section $\delta$ values of the different hybrid dyes were obtained by using *Z*-scan technique, those demonstrate the order Me + $CH_2CH_2OH$ > 2Bu > 2Pr > 2Et, as shown in Table 5. And the corresponding iodides are also listed in the Table 5 to compare with the polyoxometalates ($Mo_6O_{19}^{2-}$), a similar trend, indicating that the TPA cross sections of the polyoxometalates are larger than those of the corresponding iodide analogues.

## 4. Conclusions

Four high thermal stable hybrid inorganic-organic materials were obtained by means of metathesis approach from reaction of the four organic dyes with polyoxometalates in high yield, and characterized by single crystal X-ray diffraction analysis.

In dilute solutions, the wavelengths and fluorescent intensity of the different hybrids could be ordered according to their different substituted amino group. The longer are the alkyl group, the stronger ability the donor at our present work. However, the donor ability does not play the crucial role for the properties in solid or high concentrations. Sometimes, hydrogen bonds take drastic influence on their properties. Hybridization of polyoxometalate with organic dye leads to enhancement of thermal stability and TPA cross sections. We expect that the results can offer a reference in designing and synthesizing novel kinds of TPA materials

## Supplementary material

Crystallographic date reported in this paper has been deposited with the Cambridge Crystallographic Date Center, CCDC No. 618508 for **POM1**, No. 618510 for **POM2** and No. 618509 for **POM4**. Copies of these information may be obtained free of charge from the Director, CCDC, 12 Union Road, Cambridge CB2 1EZ, UK (fax: +44-1223/336-033; e-mail: deposit@ccdc.cam.ac.uk).

## Acknowledgments

The work was supported by a grant for the National Natural Science Foundation of China (20771001, 20875001), Education Committee of Anhui Province (KJ2010A030), Team for Scientific Innovation Foundation of Anhui Province (2006KJ007TD).

## References

[1] Mayer MG. Ueber elementarakte mit zwei quanenspruengen. Annals of Physics 1931;9:273–94.
[2] Kim HM, Cho BR. Two-photon materials with large two-photon cross sections. Structure–property relationship. Chemical Communication 2009;2:153–64.
[3] Oliveira SL, Correa DS, Misoguti L, Constantino CJL, Aroca RF, Zilio SC, et al. Perylene derivatives with large two-photon-absorption cross-sections for application in optical limiting and upconversion lasing. Advanced Materials 2005;17:1890–3.
[4] Charlot M, Izard N, Mongin O, Riehl D, Blanchard-Desce M. Optical limiting with soluble two-photon absorbing quadrupoles: structure-property relationships. Chemical Physics Letters 2006;417:297–302.
[5] Bouit PA, Wetzel G, Berginc G, Loiseaux B, Toupet L, Feneyrou P, et al. Near IR nonlinear absorbing chromophores with optical limiting properties at telecommunication wavelengths. Chemistry of Materials 2007;19:5325–35.

[6] Kim HM, Jung C, Kim BR, Jung SY, Hong JH, Ko YG, et al. Environment-sensitive two-photon probe for intracellular free magnesium ions in live tissue. Angewandte Chemie International Edition 2007;46:3460–3.
[7] Kim HM, Kim BR, Hong JH, Park JS, Lee KJ, Cho BR. A two-photon fluorescent probe for calcium waves in living tissue. Angewandte Chemie International Edition 2007;46:7445–8.
[8] Kim HM, Yang PR, Seo MS, Yi JS, Hong JH, Jeon SJ, et al. Magnesium ion selective two-photon fluorescent probe based on a benzo[h]chromene derivative for in vivo imaging. Journal of Organic Chemistry 2007;72:2088–96.
[9] Morales AR, Schafer-Hales KJ, Marcus AI, Belfield KD. Amine-reactive fluorene probes: synthesis, optical characterization, bioconjugation, and two-photon fluorescence imaging. Bioconjugate Chemistry 2008;19:2559–67.
[10] Jhaveri SJ, McMullen JD, Sijbesma R, Tan LS, Zipfel W, Ober CK. Direct three-dimensional microfabrication of hydrogels via two-photon lithography in aqueous solution. Chemical of Materials 2009;21:2003–6.
[11] Park SH, Yang DY, Lee KS. Two-photon stereolithography for realizing ultra-precise threedimensional nano/microdevices. Laser & Photonicas Reviews 2009;3:1–11.
[12] Zijlstra1 P, Chon1 JWM, Gu1 M. Five-dimensional optical recording mediated by surface plasmons in gold nanorods. Nature 2009;459:410–3.
[13] Lohse B, Vestberg R, Ivanov MT, Hvilsted S, Berg RH, Hawker CJ, et al. Acridizinium-substituted dendrimers as a new potential rewritable optical data storage material for blu-ray. Chemistry of Materials 2008;20:6715–20.
[14] O'Connor NA, Berro AJ, Lancaster JR, Gu X, Jockusch S, Nagai T, et al. Toward the design of a sequential two photon photoacid generator for double exposure photolithography. Chemistry of Materials 2008;20:7374–6.
[15] Zhou W, Kuebler SM, Carrig D, Perry JW, Marder SR. Efficient photoacids based upon triarylamine dialkylsulfonium salts. Journal of America Chemistry Society 2002;124:1897–901.
[16] Velusamy M, Shen JY, Lin JT, Lin YC, Hsieh CC, Lai CH, et al. A new series of quadrupolar type two-photon absorption chromophores bearing 11, 12-Dibutoxydibenzo[a, c]-phenazine bridged amines; their applications in two-photon fluorescence imaging and two-photon photodynamic therapy. Advanced of Function Materials 2009;19:2388–97.
[17] Peter CF. Polychromophoric metal complexes for generating the bioregulatory agent nitric oxide by single- and two-photon excitation. Accounts of Chemical Research 2008;41:190–200.
[18] Jiang YQ, Horimoto NN, Imura K, Okamoto H, Matsui K, Shigemoto R. Bio-imaging with two-photon-induced luminescence from triangular nanoplates and nanoparticle aggregates of gold. Advanced Materials 2009;21:2309–13.
[19] Koo CK, Wong KL, Man CWY, Lam YW, So LKY, Tam HL, et al. A bio-accumulative cyclometalated platinum(II) complex with two-photon-induced emission for live cell imaging. Inorganic Chemistry 2009;48:872–8.
[20] Chung SJ, Perry JW, Marder SR. Strong, low-energy two-photon absorption in extended amine-terminated cyano-substituted phenylenevinylene oligomers. Journal of America Chemistry Society 2005;127:10844–5.
[21] Krishna TR, Parent M, Werts MHV, Blanchard-Desce M. Water-soluble dendrimeric two-photon tracers for in vivo imaging. Angewandte Chemie International Edition 2006;45:4645–8.
[22] Chung SJ, Zheng SJ, Odani T, Bredas JL, Perry JW, Marder SR, et al. Extended squaraine dyes with large two-photon absorption cross-sections. Journal of America Chemistry Society 2006;128:14444–5.
[23] He GS, Tan LS, Zheng QD, Prasad PN. Multiphoton absorbing materials: molecular designs, characterizations, and applications. Chemical Review 2008;108:1245–330.
[24] Lancaster K, Odom SA, Jones SC, Thayumanavan S, Marder SR, Barlow S, et al. Intramolecular electron-transfer rates in mixed-valence triarylamines: measurement by variable-temperature ESR spectroscopy and comparison with optical data. Journal of American Chemistry Society 2009;131:1717–23.
[25] Pawlicki M, Collins HA, Denning RG, Anderson HL. Two-photon absorption and the design of two-photon dyes. Angewandte Chemie International Edition 2009;48:3244–66.
[26] Wampler RD, Moad A, Moad C, Heiland R, Simpson G. Visual methods for interpreting optical nonlinearity at the molecular level. Accounts of Chemical Research 2007;40:953–60.
[27] Sullivan P, Dalton L. Theory-Inspired development of organic electro-optic materials. Accounts of Chemical Research 2010;43:10–8.
[28] Marder SRJ, Perry W, Schaefer WP. Synthesis of organic salts with large second-order optical nonlinearities. Science 1989;245:626–8.
[29] Marder SR, Perry JW, Tiemann BG, Warsh RE, Schaefer WP. Second-order optical nonlinearities and photostabilities of 2-N-methylstilbazolium salts. Chemistry of Materials 1990;2:685–90.
[30] Geskin V, Lambert C, Bredas J. Origin of high second- and third-order nonlinear optical response in ammonio/borato diphenylpolyene zwitterions: the remarkable role of polarized aromatic groups. Journal of American Chemistry Society 2003;125:15651–5.
[31] Koleva BB, Kolev T, Seidel RW, Mayer-Figge H, Spiteller M, Sheldrick WS. On the origin of the color in the solid state. crystal tructure and optical and magnetic properties of 4-cyanopyridinium hydrogensquaratSe monohydrate. Journal of Physical Chemistry A 2008;112:2899–905.
[32] Kolev T, Koleva BB, Spiteller M, Mayer-Figge H, Sheldrick WS. The crystal structure and optical properties of 1-methyl-4-[2-(4-hydroxyphenyl)ethenyl] pyridinium dihydrogenphosphate: new aspects on crystallographic disorder and its effect on polarized solid-state IR spectra. Dyes and Pigments 2008;79:7–13.
[33] Koleva BB, Kolev T, Seidel RW, Spiteller M, Mayer-Figge H, Sheldrick WS. Self-assembly of hydrogensquarates: crystal structures and properties. Journal of Physical Chemistry A 2009;113:3088–95.
[34] Kolev T, Tsanev T, Kotov S, Mayer-Figge H, Spiteller M, Sheldrick WS, et al. Anyles of 4-benzoylpyridine-Crystal structure and spectroscopic properties. Dyes and Pigments 2009;82:95–101.
[35] Ivanova B, Spiteller M. Noncentrosymmetric crystals with marked nonlinear optical properties. Journal of Physical Chemistry A 2010;114:5099–103.
[36] Ivanova B, Spiteller M. Possible application of the organic barbiturates as NLO materials. Crystal Growth & Design 2010;10:2070–4.
[37] Zhang J, Song YF, Cronin L, Liu TB. Self-assembly of organic–inorganic hybrid amphiphilic surfactants with large polyoxometalates as polar head groups. Journal of America Chemistry Society 2008;130:14408–9.
[38] Kida N, Hikita M, Kashima I, Okubo M, Itoi M, Enomoto M, et al. Control of charge transfer phase transition and ferromagnetism by photoisomerization of spiropyran for an organic–inorganic hybrid system, (SP)[$Fe^{II}Fe^{III}$(dto)$_3$] (SP = spiropyran, dto = $C_2O_2S_2$). Journal of American Chemistry Society 2009;131:212–20.
[39] Coe B. Switchable nonlinear optical metallochromophores with pyridinium electron acceptor groups. Accounts of Chemical Research 2006; 39:383–93.
[40] Zhang XJ, Tian YP, Jin F, Wu JY, Xie Y, Tao XT, et al. Self-assembly of an organic chromophore with Cd-S nanoclusters: supramolecular structures and enhanced emissions. Crystal Growth & Design 2005;5:565–70.
[41] Tian YP, Li L, Zhou YH, Wang P, Zhou HP, Wu JY, et al. Design and synthesis of two new two-photon absorbing pyridine salts as ligands and their rare earth complexes. Crystal Growth & Design 2009;9:1499–504.
[42] Hao FY, Zhang XJ, Tian YP, Zhou HP, Li L, Wu JY, et al. Design, crystal structures and enhanced frequency-upconverted lasing efficiencies of a new series of dyes from hybrid of inorganic polymers and organic chromophores. Journal of Material Chemistry 2009;19:9163–9.
[43] Coronado E, Gómez-García CJ. Polyoxometalate-based molecular materials. Chemical Review 1998;98:273–96.
[44] Coronado E, Gómez-García CJ. Polycxometalates: from magnetic clusters to molecular materials. Comments Inorganic Chemistry 1995;17:255–81.
[45] Coronado E, Delhaes P, Galán-Mascarós JR, Giménez-Saiz C, Gómez-García CJ. Hybrid molecular materials having conducting and magnetic networks: charge transfer salts based on organic [pi]-donor molecules and inorganic magnetic clusters. Synthetic Metals 1997;85:1647–50.
[46] Yang WJ, Kim DY, Kim CH, Jeong MY, Lee SK, Jeon SJ, et al. Triphenylamine derivatives with large two-photon cross-sections. Organic Letters 2004;6: 1389–92.
[47] Marder SR, Perry JW, Yakymyshyn CP. Organic salts with large 2nd-order optical nonlinearities. Chemistry of Materials 1994;6:1137–47.
[48] Grabowski ZR, Rotkiewicz K, Rettig W. Structural changes accompanying intramolecular electron transfer: Focus on twisted intramolecular charge-transfer states and structures. Chemical Review 2003;103:3899–4032.
[49] Sheldrick GM. SHELXL-97, program for crystal structures refinement. Göttingen (Germany): University of Göttingen; 1997.
[50] Marder SR, Perry JW, Bourhill G, Gorman CB, Tiemann BG, Mansour K. Relation between bond-length alternation and second electronic hyperpolarizability of conjugated organic molecules. Science 1993;261:186–9.
[51] Wang XM, Zhou YF, Yu WT, Wang C, Fang Q, Jiang MH, et al. Two-photon pumped lasing stilbene-type chromophores containing various terminal donor groups: relationship between lasing efficiency and intramolecular charge transfer. Jounral of Materials Chemistry 2000;10:2698–703.
[52] McQuade DT, Kim JS, Swager TM. Two-Dimensional conjugated Polymer Assemblies: interchain Spacing for Control of Photophysics. Journal of American Chemistry Society 2000;122:5885–6.
[53] Hua ZJ, Sun PP, Li L, Tian YP, Yang JX, Wu JY, et al. Two novel p-conjugated carbazole derivatives with blue two-photon-excited fluorescence. Chemical Physics 2009;355:91–8.
[54] Brittain HG. Solid-state fluorescence of the trihydrate phases of ampicillin and amoxicillin. AAPS PharmSciTech 2005;6:444–8.
[55] Kolev T, Koleva BB, Seidel RW, Spiteller M, Sheldrick WS. New aspects on the origin of color in the solid state. coherently shifting of the protons in violurate crystals. Crystal Growth & Design 2009;9:3348–52.